Excited State Luminescence of Multi-(5-phenyl-1,3,4-oxadiazo-2-yl)benzenes in an Electron-Donating Matrix: Exciplex or Electroplex?

Chih-Chiang Yang,[†] Chia-Jung Hsu,[†] Pi-Tai Chou,*[,†] Hsu Chun Cheng,[§] Yuhlong Oliver Su,*[,§,⊥] and Man-kit Leung*[,†,‡]

Department of Chemistry, Institute of Polymer Science and Engineering, National Taiwan University, 1 Roosevelt Road, Section 4, Taipei 106, Taiwan, R.O.C., Department of Applied Chemistry, National Chi Nan University, Nantou 545, Taiwan, Department of Chemistry, National Chung Hsing University, Taichung 402, Taiwan

Received: September 28, 2009; Revised Manuscript Received: November 25, 2009

Multi-(5-phenyl-1,3,4-oxadiazo-2-yl)benzenes show emission in organic solvents from ultraviolet to blue (339−447 nm). The reduction potentials $E_{1/2}^{red}$ cover a large range of −2.11 V for 2,5-diphenyl-1,3,4-oxadiazole to −0.76 V for 1,2,3,4,5,6-hexa(5-phenyl-1,3,4-oxadiazo-2-yl)benzene. An unexpectedly wide spectral range of the oxadiazole (OXD) exciplex emissions in PVK is observed, ranging from 406 to 603 nm. The OXDs also exhibit similar electroluminescence (EL) when blended into polyvinylcarbazole (PVK). A linear correlation between the λ_{max} of the electroluminescence and photoluminescence is observed, implying that the emission mechanisms in both processes are similar. In addition, the linear correlation between the $E_{1/2}^{red}$ versus λ_{max} of EL (eV) reflected that the term of the charge-transfer configuration of the contact electron−hole pair plays a major role in the exciplex emission. The exciplex EL of 1,2,5-tri(5-phenyl-1,3,4-oxadiazo-2-yl)benzene (**5**) could be as high as 1.0 cd/A. Since the exciplex emission usually has a large Stokes shift, this provides a window for us to generate duo emissions for near white light EL with high efficiency. Among the devices we tried, the device of PVK/2-*tert*-butylphenyl-5-biphenyl-1,3,4-oxadiazole/**5**/2,5,8,11-tetra-*tert*-butylperylene (100:40:40:4) gave EL with good current efficiency of 1.63 cd/A.

Introduction

Since the successful fabrication of the first high-brightness organic light emitting diode (OLED),[1] thin-film OLEDs based on small molecules[1,2] or polymer[3] have attracted a lot of attention due to their great potentials on the technologies of the large-scale, full-color, flat-panel display and the back-illuminated liquid crystal display.[4] Device structures such as a multilayer discrete structure,[5] or single a layer structure with balanced hole and electron transport properties have been developed.[6,7] Among these OLEDs, several different kinds of light-emitting mechanisms, including fluorescence or phosphorescence from excitons, excimers, electromers, electroplexes, or exciplexs have been reported.[8,9]

Recently, OLED research based on excited state complexes has attracted a lot of attention. Exciplex is considered as one kind of excited state complexes that is formed by an electronically excited state donor molecule, D* (or acceptor A*), with a complementary acceptor molecule, A (or donor D), in their ground state. In theory, the donor−acceptor pair constitutes an exciplex with an average separated distance of 0.3−0.4 nm.[10] The exciplex is composed of partially charged components ($0 < \delta < 1$) with limited extents of charge separation between the donor−acceptor pair. The exciplex emission is usually weak and shows poor performance of OLED.[8,9] However, the studies on enhanced exciplex emission of polymer systems suggested the possibility of using LED devices as a broadband emission source.[8a,9f,g]

In contrast to the emission theory of exciplexes, the phenomenon of electroplex emission[10] has recently been reported. Electroplexes form between the complementarily charged molecules in which a hole will usually be located on an electron-donating site, and an electron, on an electron-accepting site. The donor and acceptor pair constitutes an electroplex with an average separated distance of 0.4−0.7 nm,[10c] which is relatively longer than the distance for the exciplex pair. Either formation of the electroplexes at the interface of the hole transport layer (HTL) and the electron transport layer (ETL) or in a homogeneous blend has been suggested.

Unless the dissociation process of the excited states into the separated ion pair is facile, photoexcitation rarely generates free charge carriers. Therefore, the emission signature of electroplexes is visible mostly in the electroluminescence (EL) spectrum but not normally in the photoluminescence (PL) spectrum. On the other hand, exciplex emissions are readily observed in the EL and PL processes.

Oxadiazole (OXD) molecules are among the most widely studied electron-transport materials for OLEDs.[11] Many different types of structures, including dimeric,[12] trimeric,[13] starburst,[14] and tetraphenylmethane[15]-based OXDs have recently been investigated. When OXDs have been blended in an electron-donating matrix, either formation of exciplexes or electroplexes has been reported. For example, exciplexes or electromers were observed when 2-*tert*-butylphenyl-5-biphenyl-1,3,4-oxadiazole (PBD) was blended into polyvinylcarbazole (PVK). Conversely, due to the topological constrains in the skeleton, electroplexes were evidenced in a carbazole−OXD-based copolymer.[8g]

* Corresponding authors. (M.-k.L.) Phone: +886-2-33661673. Fax: +886-2-23636359. E-mail: mkleung@ntu.edu.tw. (P.-T.C.) Phone: 886-2-3366-3894. Fax: 886-2-2369-5208. E-mail: chop@ntu.edu.tw. (Y.O.S.) Phone: 886-49-2910960 ext. 4150. Fax: 886-49-2917956. E-mail: yosu@ncnu.edu.tw.

† Department of Chemistry, National Taiwan University.

‡ Institute of Polymer Science and Engineering, National Taiwan University.

§ National Chi Nan University.

⊥ National Chung Hsing University.

10.1021/jp9093063
Published on Web 12/29/2009

SCHEME 1: Design of Multi-(5-phenyl-1,3,4-oxadiazo-2-yl)benzenes

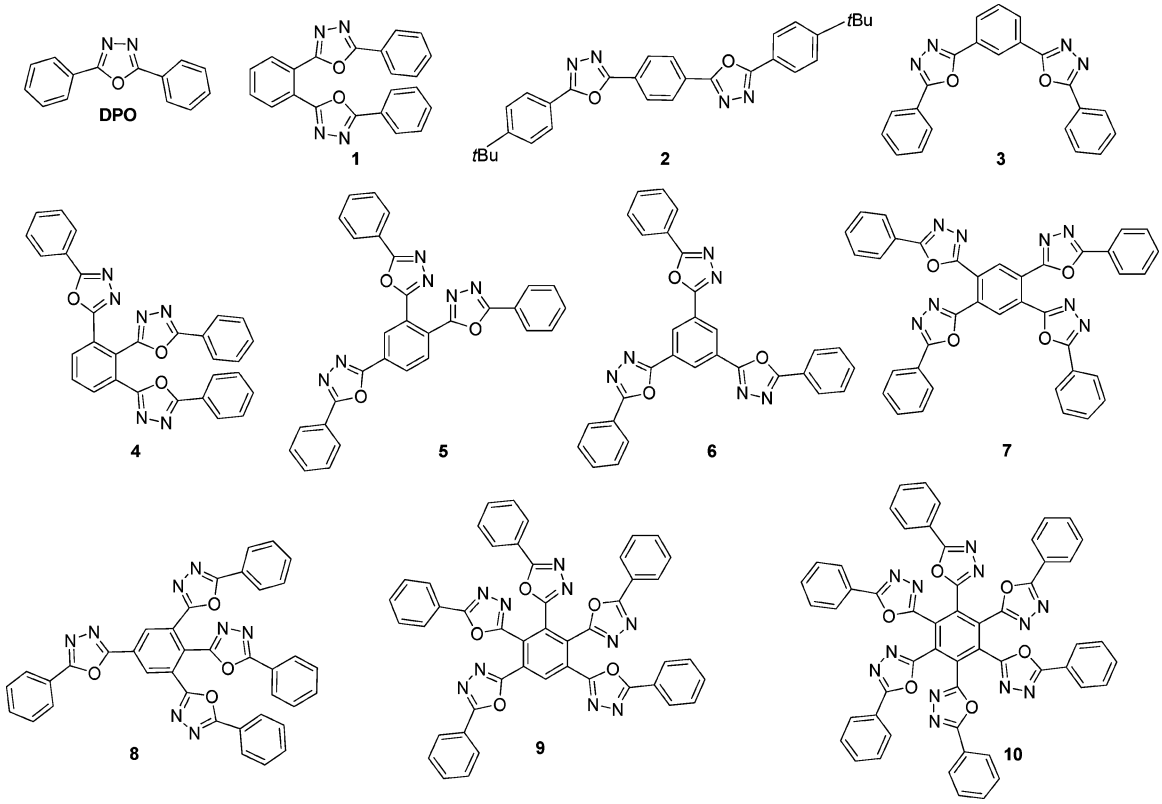

Since the charge-separation process of the excited species is not only an interesting issue in the OLED research but also an important topic in the design of organic solar cells,[9f,16,17] in the present article, we have carried out systematic studies of the exciplex formation of the oxadiazole (OXD) derivatives in PVK blends as emitter.[6b] We are highly interested in understanding whether the formation of electroplexes, other than exciplexes, could be driven by modulating the HOMO−LUMO gap between the PVK−OXD moieties. A series of multioxadiazole-substituted benzenes (Scheme 1) were therefore prepared and investigated.

PVK is an electron-rich and hole-transporting polymer with excellent film properties.[18] The photophysical and electrochemical properties, photoluminscent behavior, and electroluminescent performance have been extensively discussed in the literature.[19] In the present work, PVK was used as our workhorse to form exciplexes with the electron-deficient OXD derivatives. In addition, near white-light OLEDs with high EL efficiency based on the blending of a blue fluorescent dye and a yellow exciplex emitter were demonstrated.

Results and Discussion

Syntheses. Scheme 2 shows the synthetic approaches for the target multi(5-phenyl-1,3,4-oxadiazo-2-yl)benzene derivatives. The commercially available aryl acids, or acyl chlorides, and aryl nitriles were directly used without further purification. Other acid chlorides were synthesized on treatment of the corresponding aryl acids with PCl_5.[19] 1,2-Bis(5-tetrazolyl)benzene, 1,4-bis(5-tetrazolyl)benzene, and (5-tetrazolyl)benzene were prepared according to literature procedures.[20] The tetrazoles were prepared by treating the corresponding aryl nitriles with NaN_3 and NH_4Cl[21] in DMF. Pyromellitoyl tetrachloride was prepared from pyromellitic dianhydride and PCl_5 with addition of one drop of $POCl_3$ as promoter.[22] OXDs **1**−**5**[23] and **7**−**10** were

SCHEME 2: Syntheses of the OXD Derivatives 1−10

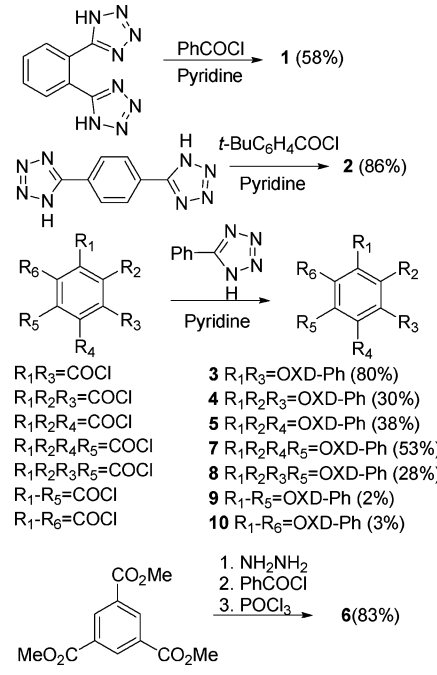

synthesized via the Huisgen reaction from the corresponding acyl chlorides.[24] Although the yields of **9** and **10** were low, they could be conveniently purified by liquid column chromatography and further recrystallization from appropriate solvents. Compound **2**[12a] was prepared by reacting 1,4-bis(5-tetrazolyl)benzene with 4-*tert*-butylbenzoyl chloride in pyridine.[20a] Introduction of the *tert*-butyl groups at both ends of **2** is necessary to obtain a sample with reasonable solubility. The synthesis of **6** was started from benzene-1,3,5-tricarboxylic acid trimethyl ester and adopted

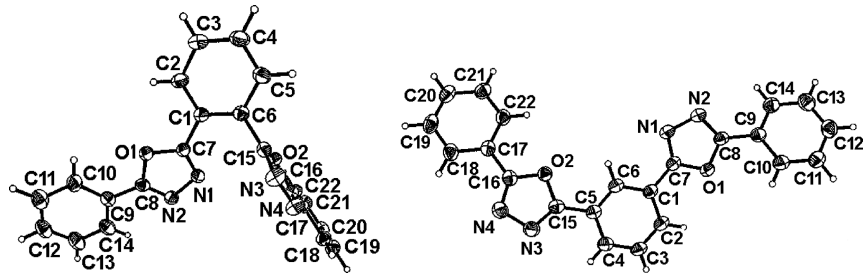

Figure 1. ORTEPs of **1** (left) and **3** (right).

TABLE 1: Photophysical Properties of the OXD Derivatives 1−10 in Solution

	UV−vis absorption[a]	fluorescence[a]	
OXD	λ_{max}, nm ($\varepsilon \times 10^{-4}$)	λ_{max}, nm (Stokes Shift, nm)	quantum yield[b]
1	289 (2.44)	382 (93)	0.83
2	321 (5.60)	380 (59)	0.96
3	286 (5.39)	339 (53)	0.75
4	289 (2.33)	418 (129)	0.29
5	318 (2.18)	391 (73)	0.74
6	294 (9.50)	360 (66)	0.43
7	290 (2.33), 333 (1.58)	411 (78)	0.53
8	300 (6.14)	427 (127)	0.21
9	307 (7.14)	428 (121)	0.094
10	314 (3.77)	447 (133)	0.019
PBD	306 (2.58)	365 (59)	0.84
DPO	283 (2.18)	346 (63)	0.45

[a] Measured in $CHCl_3$. [b] Quantified in THF against coumarin 1 (quantum yield: 0.85)[34] as standard.

a reaction sequence of hydrazide formation, acylation, and dehydration to give **6** in 83% overall yield.[25]

X-ray Crystallographic Characterization of 1 and 3. Single crystals of **1** and **3** were prepared from MeOH and PhMe, respectively. In the single crystal, **1** adopts a nonplanarized conformation with an OXD ring aligned orthogonally to the other (Figure 1). Although the first OXD ring is almost coplanar with the central 1,2-phenylene group with a dihedral angle of 23.8° ($C_6-C_1-C_7-N_1$), the second OXD ring is rotated by a torsional angle of 85.0° ($C_1-C_6-C_{15}-N_3$) about the OXD ring and the neighboring 1,2-phenylene group. OXD **3** adopts, on the other hand, an almost fully coplanar conformation with the two dihedral angles of the OXD ring and the central 1,3-phenylene group of 9.8° ($C_6-C_1-C_7-N_1$), 11.1° ($C_4-C_5-C_{15}-N_3$). The conformation of **1** is probably governed by the steric repulsion between two OXD rings, which could be significantly reduced by keeping the rings at orthogonal positions. In addition, the proximity of the OXD rings might allow the through-space electronic interactions, with the nitrogen lone-pair electrons on the first OXD ring donating to the other electron-deficient OXD π-system.

UV−vis Absorption Properties. A brief summary of the photophysical data for **1**−**10** in $CHCl_3$ is listed in Table 1. Their UV absorption spectra are shown in Figure 2. Herein, we adopt 2,5-diphenyloxadiazole (DPO) as our reference for comparison. The UV−vis spectra of all OXDs exhibit intense UV absorption bands ($\varepsilon \sim 10^4$ M^{-1} cm^{-1}) due to the spin-allowed $\pi-\pi^*$ transitions in the singlet manifold ranging from 250 to 350 nm. DPO, the reference, has an absorption λ_{max} at 283 nm. The meta-conjugated **3** and **6** show small shifts of the λ_{max} with respect to DPO by 3 and 11 nm, reflecting that the meta-conjugation effects on their ground state are weak. The ortho-substituted **1** and **4** also show a small shift by 6 nm with respect to DPO, which is quite unexpected at the beginning; The ortho π-systems

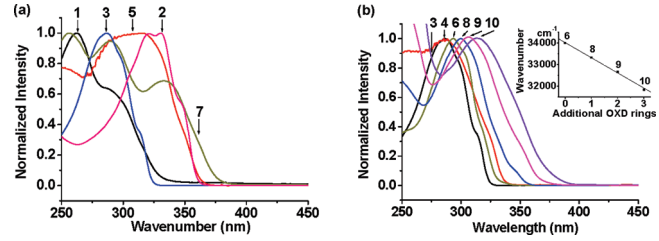

Figure 2. UV absorption spectra of the OXD derivatives. Spectra of (a) **1**−**3**, **5**, and **7** and (b) **3**, **4**, **6**, and **8**−**10**.

are, generally speaking, supposed to be conjugative and are expected to have significant spectral red shift due to the π-conjugation. However, our X-ray crystallographic data of **1** reveal that the ortho-π-conjugation is interrupted by the non-planarized and almost orthogonal conformation; one coplanar OXD moiety conjugated with the central benzene ring would show DPO-like chromophoric absorption, and the other one aligned perpendicularly would lead to only small perturbations on the spectrum. Recently, there has been a lot of attention paid to the discussions of cruciforms, which show disjoint FMO structures even when the π-systems are linked in ortho positions.[26]

On the other hand, the para-substituted **2** is expected to be coplanar. The strong π-electronic couplings lead to a significant red shift on the spectrum, which shows the λ_{max} at 321 nm (Figure 2a). The absorption of **5** is broad, on the other hand, covering the absorption ranges of **2** and **3**. The λ_{max} of 318 nm is slightly blue-shifted in comparison to that of **2**. This is because the OXD rings are not fully planarized with each others due to the steric repulsions between the ortho-substituents, and therefore, the π-conjugation is reduced. The absorption spectrum of **7** shows splitting bands peaking at 290 and 333 nm, respectively. The band at 333 nm might arise mainly from the $\pi-\pi^*$ transition of the para-conjugated OXD chromophores, whereas the band at 290 nm might arise mainly from the electronic transitions of the meta-OXD chromophores.

As mentioned before, probably due to the steric-hindrance reason, the absorption of **6** (λ_{max} = 294 nm), **8** (λ_{max} = 300 nm), **9** (λ_{max} = 307 nm), and **10** (λ_{max} = 314 nm) are all blue-shifted with respect to that of **2** and **5** (Figure 2b). However, the trend of gradually red-shifted absorptions of **6**, **8**, **9**, and **10** from 294 to 314 nm could not be fully explained by this reason; on the basis of the steric point of view, one might expect that the highly sterically hindered **10** should be the most blue-shifted one due to the lowest degree of planarization of the substituents, which contradicts the observations. Therefore, other factors such as substituent electronic effects must have some roles on the spectral red-shift phenomena. The inset of Figure 2b shows a linear correlation between the $1/\lambda_{max}$ and the number of additional OXD rings onto the 1,3,5-substituted core. We attribute these observations to the substituent inductive effects that stabilize the LUMO level of the 1,3,5-substituted core; the

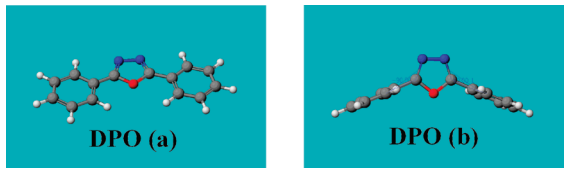

Figure 3. PM5 calculations of DPO: (a) fully coplanar conformation and (b) conformation with the phenyl groups aligned perpendicularly to the OXD ring.

LUMO of **8**−**10** would therefore gradually descend due to the additional inductive effects from the electron-withdrawing OXD substituents, leading to the spectral red shift with respect to **6**. This suggestion is further supported by the electrochemical data that will be discussed in a later section.

Conformational Analysis. Semiempirical PM5 calculations were employed to assist our conformational analysis.[27] The results are depicted as follows with O in red, N in blue, C in black, and H in white. Our calculations reveal that the planarized conformation of DPO is 2.9 kcal/mol more stable than the orthogonal one, indicating that the π-conjugation effects between the phenyl rings and the OXD units are significant (Figure 3).

Similarly, our calculations suggest that the planar forms of **3a** and **3b** (Figure 4), with an estimated heat of formation of 101.9 kcal/mol for both, are more stable than **3c** by 1.2 kcal/mol and than **3d** by 1.7 kcal/mol. These results are again in good agreement with the X-ray diffraction data.

Due to the lack of the steric hindrance, our calculations also predict that 1,3,5-substituted **6** should possess coplanar conformations (Figure 5). The coplanar forms of **6a** and **6b** have the lowest estimated heat of formation in comparison to the other conformations. Therefore, the OXD rings tend to maintain the coplanar alignment with the central ring to optimize the π-conjugation. However, the calculated heat of formation of 144.9 kcal/mol for **6b** was found to be slightly higher than that of 144.0 for **6a**.

When an additional OXD unit is placed at the 2-position of **6** to form **8**, the fully coplanar alignment becomes unfavorable due to steric congestion (Figure 6). To minimize the steric repulsions between the substituents and to maintain the highest conjugation stabilization, the additional OXD ring is locked at the perpendicular position while the other three OXD groups at the 1, 3, and 5 positions are almost planarized with respect to the central benzene ring. Nevertheless, our calculations reveal that the OXD rings at the 1 and 3 positions are slightly tilted to avoid the steric repulsions. The conformer **8a**, with two oxygen atoms pointing toward the perpendicular 2-OXD ring, has an estimated heat of formation of 190.4 kcal/mol that is more stable than **8b** by 0.7 kcal/mol and than **8c** by 3.1 kcal/mol. On the other hand, if the 2-OXD ring is kept at the coplanar position, the OXD rings at the 1 and 3 positions would therefore be tilted significantly so that they are no longer conjugated with the central ring in **8d**. Thus, conformer **8d** is found to be 2.1 kcal/mol higher than that of **8a**. The inset of Figure 2b shows a linear correlation between the $1/\lambda_{max}$ and the number of additional OXD rings onto the 1,3,5-substituted core, indicating that similar situations are likely to occur also on **9** and **10**. Since the LUMO levels of **8**−**10** gradually descend due to the additional inductive effect from the OXD substituents, the spectral red shift with respect to **6** would therefore result.

Photoluminescent Behavior. The photoluminescent data are shown in Table 2 and Figure 7. Fluorescence from **1**−**10** in $CHCl_3$ appears in the range of 340−450 nm. Among the OXDs we studied, two classes of OXD compounds based on their

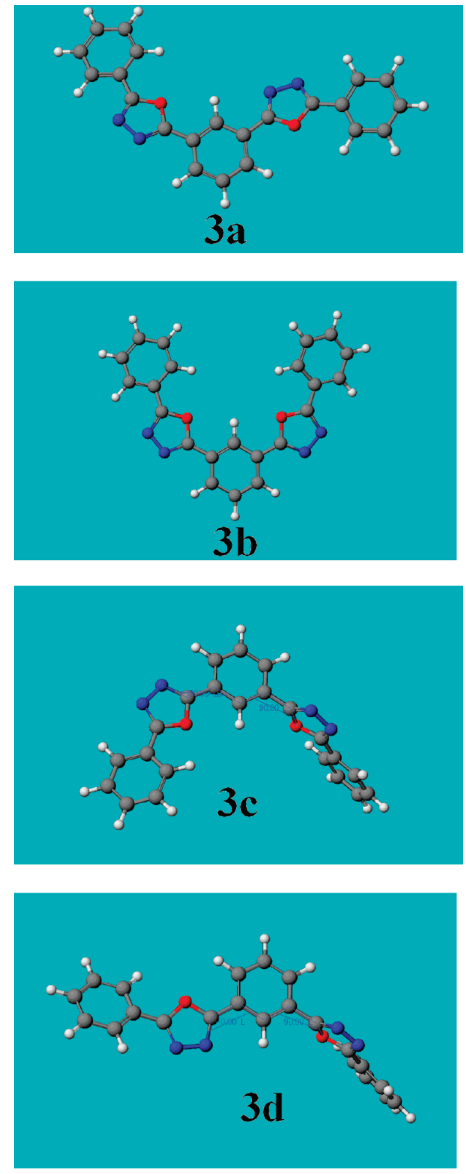

Figure 4. PM5 calculated conformers of **3a**−**3d**.

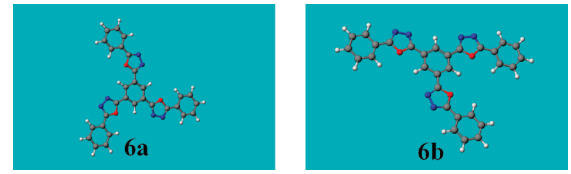

Figure 5. PM5 calculated conformers of **6a** and **6b**.

fluorescent behaviors have been identified: (1) the para- and meta-substituted **2**, **3**, and **6** which show vibronic fine pattern with small Stokes shifts ranging from 50−66 nm (Figure 7a) and (2) the ortho-substituted OXD derivatives **1**, **4**, **5**, and **7**−**10**, which show structureless emission with large Stokes shifts ranging from 73 to 133 nm (Figure 7b). All their room-temperature emission spectra are quite different from the mirror images of their lowest-energy absorption band with modestly large Stokes shifts, indicating that the geometry of **1**−**10** in their relaxed Franck−Condon excited state is different, to a certain extent, from that of their ground state. The geometrical differences may arise either from the bond-rotational or from the vibrational relaxations, depending on the ground state geometry of the OXD molecules.

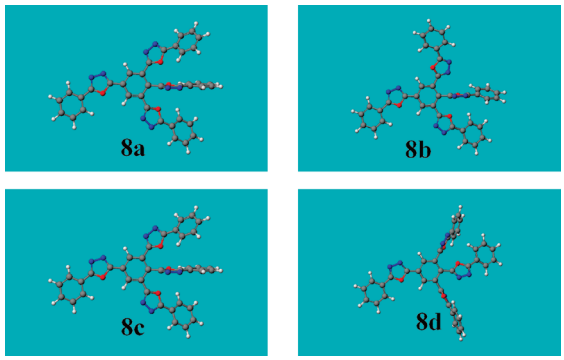

Figure 6. PM5 calculated conformers of **8a**−**8d**.

TABLE 2: Electrochemical Reduction Potentials, Optical Band Gaps, and Estimated HOMO/LUMO Levels of 1−10

	$E_{1/2}^{red}$ [a] (V)			energy level (eV)		
OXD	E_1	E_2	E_3	LUMO[c]	band gap[d]	HOMO[e]
1	−1.54	−1.97	−2.14	−2.68	3.76	−6.44
2	−1.52	−1.97		−2.70	3.44	−6.14
3	−1.80	−2.12		−2.42	3.83	−6.25
4	−1.65	−1.86		−2.57	3.65	−6.22
5	−1.34	−1.85		−2.88	3.40	−6.28
6	−1.53			−2.69	3.76	−6.45
7	−1.05	−1.61		−3.17	3.30	−6.47
8	−1.22	−1.55[b]		−3.00	3.55	−6.55
9	−0.96			−3.26	3.39	−6.65
10	−0.76	−1.31	−1.68	−3.46	3.29	−6.75
PBD	−1.95			−2.27[f]	3.60	−5.87
DPO	−2.11	−2.48		−2.11	3.87	−5.98

[a] By CV in THF, with Bu_4NClO_4 (0.1 M) as supporting electrolyte vs Ag/AgCl. The scan rate was 100 mV/s. [b] Irreverisable wave. [c] LUMO = $-(E_1 - 0.58) - 4.8$ (eV). [d] Band gap = 1240.8/Abs.λ_{onset} (nm). [e] HOMO = LUMO − band gap (eV). [f] PBD with an EA of 2.16 eV and an IP of 6.06 eV were reported in the literature.[28a]

Emission Behavior of the Para and Meta-Substituted 2, 3, and 6. DPO, our standard model, emits at 346 nm with a Stokes shift of 63 nm (Figure 7a). The vibronic progression of 1506 cm^{-1} has been clearly observed in the spectrum, suggesting that the σ-bond rotational relaxation in the Franck−Condon excited state is small. Since DPO has a conjugative coplanar ground state, the coplanar conformation would still be maintained in the relaxed Franck−Condon excited state. However, even their Stokes shifts are modest: the main vibronic band of the emission spectrum is no longer the 0,0 transition and might correspond to the vibronic 0,1 transition.

Comparing to DPO, **3** and **6** demonstrate similar vibronic patterns, as well, in their spectra. Whereas **3** shows photoemission peaking at 339 nm with a Stokes shift of 53 nm, **6** demonstrates a red-shifted emission peaking at 360 nm with a similar Stokes shift of 66 nm. Clear vibronic progressions of 1462 and 1376 cm^{-1}, respectively, have been recorded. Probably due to the increased conjugation, the vibronic progressions are smaller than that of DPO. The similarity of their fluorescent behaviors suggests that their fluorophores are highly DPO-like. Similar to that of DPO, the main band of the emission spectra is again no longer the 0,0-transition and might correspond to the vibronic 0,1 transition. These results again reflect that vibrational relaxation with respect to the ground state would also occur in the Franck−Condon excited state. The para-conjugated **2**, on the other hand, shows a significantly red-shifted emission peaking at 380 nm, with a similar Stokes shift of 59 nm and vibronic progression of 1461 cm^{-1}.

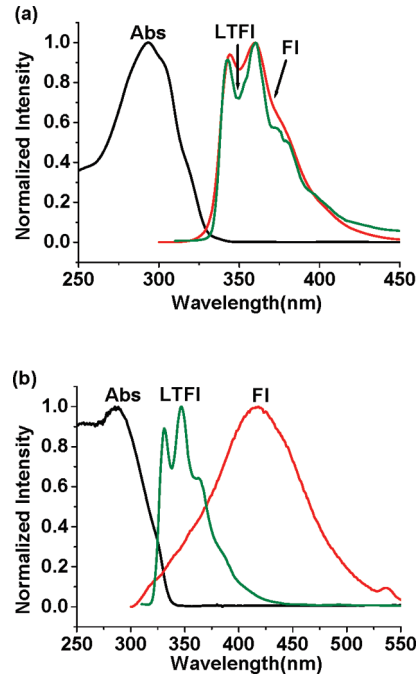

Figure 8. UV absorption spectra, room-temperature fluorescence spectra (F1), and low-temperature fluorescence spectra (LTF1) of (a) **6** and (b) **4**.

It is noteworthy to mention that the low-temperature fluorescent spectra of DPO, **2**, **3**, and **6** in a glassy organic matrix at 77 K are also well-structured with a sharper line shape. The patterns and the λ_{max} are almost identical to their room-temperature fluorescent spectra in solution. Spectra of **6** are selected as examples for illustration in Figure 8a. Since the σ-bond rotational motions are presumed to be largely frozen in an organic glassy matrix at low temperature, the observation of the almost identical fluorescence spectra either in solution at

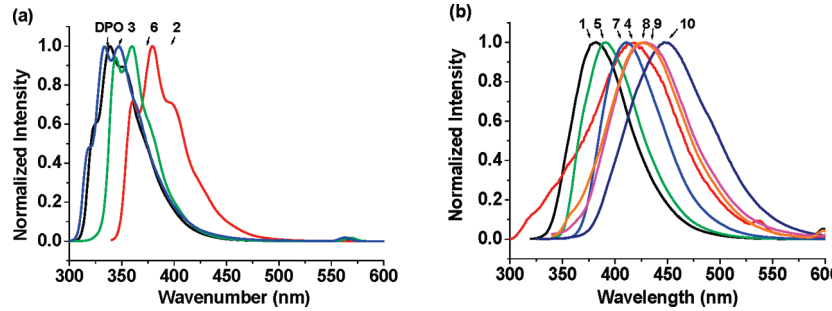

Figure 7. Photoluminescence spectra of OXD derivatives in $CHCl_3$ solution. Emission spectra of (a) DPO, **2**, **3**, and **6** and (b) **1**, **4**, **5**, and **7**−**10**.

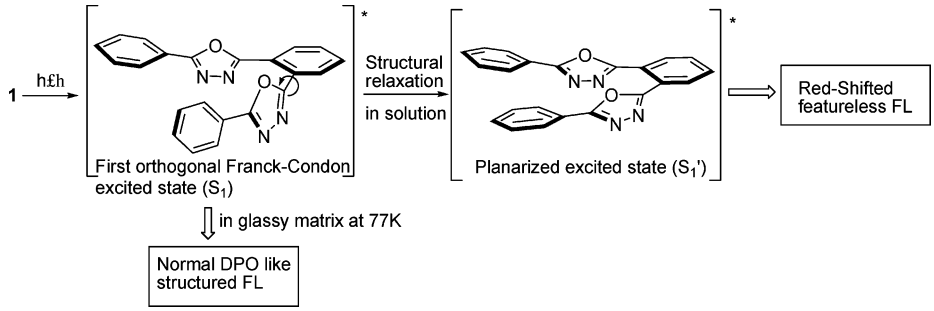

Figure 9. Structural relaxation pathways after photoexcitation.

room temperature or in an organic glass matrix at low temperature implies that freezing of the σ-bond rotational relaxation does not significantly affect the structural relaxation of the Franck−Condon excited state.

Emission Behavior of the Ortho-Substituted 1, 4, 5, and 7−10. On the other hand, all ortho-conjugated derivatives **1**, **4**, **5**, and **7−10** show broad and featureless emission with the band gradually red-shifted, in comparison to that of DPO, by a range of 34−111 nm (Table 1). Example spectra of **4** are selected and illustrated in Figure 8b for discussion. The large Stokes shifts spanning a wide range of 73−133 nm are characteristic of this class of molecules. Although in some other cases, the Stokes shifts are highly solvent-dependent, the insignificant solvent polarity effects in our cases indicate that the featureless broad emission does not arise from the charge transfer character in the excited state followed by solvent-reorganization process. We therefore presume that the structural relaxation pathway of the Franck−Condon excited state of the ortho-conjugated OXDs is different from that of the para- and meta-OXDs. Conversely, the normal DPO-like emissions, with fine vibronic patterns, are resumed when the emission spectra are collected at 77 K in an glassy organic matrix. The spectra are well-structured with the emission λ_{max} significantly blue-shifted. We explain the red-shifted emissions as a consequence of coplanarization of the ortho-OXD units after photoexcitation: When the noncoplanarized OXD molecules are excited at 77 K, emission from the nonplanarized excited state is predominant due to the restriction of the σ-bond rotational relaxation in a glassy matrix. In contrast, relaxation of the nonplanarized Franck−Condon excited state at room temperature to a flattened geometry is facile. Emissive transition from this relaxed Franck−Condon excited state would give rise to a red-shifted and featureless emission band. This approach has been adopted by Doroshenko's group to explain the photophysical behavior of 1,2-bis(5-phenyloxazol-2-yl)benzene.[28] A schematic diagram is shown in Figure 9. After photoexcitation, the Franck−Condon excited state of **1** would evolve from the nonplanarized S_1 state, to the planarized excited state S_1' that leads to the large Stokes shift of 93 nm in the emission spectrum.

This could explain the unusually large Stokes shifts for **4** and **8−10** in solution. The emission of the multi-OXD derivatives spans a wide region from ultraviolet to blue, meaning that the energy of the excited state decreased by increasing the number of OXD units. More interestingly, the quantum yields also drop dramatically when the sizes of the ortho arrays increase. The descending order of the quantum yields of **1** (0.83), 1,2,3-substituted **4** (0.29), 1,2,3,5-substituted **8** (0.21), 1,2,3,4,5-substituted **9** (0.095), and 1,2,3,4,5,6-substituted **10** (0.019) was found according to our measurements. These results again indicate that the probability of the emission from the flattened excited state back to the perpendicular ground state is low and is probably subject to σ-bond rotational types of radiationless deactivation.

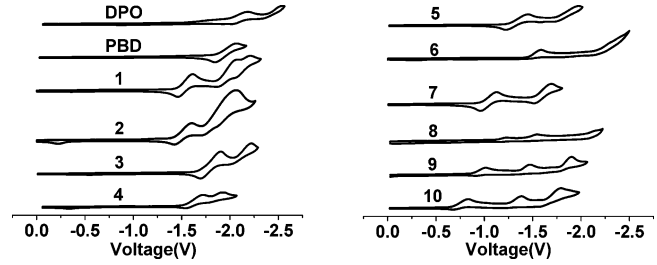

Figure 10. Cyclic voltammograms for **DPO**, **PBD**, and OXDs **1−10** under N_2 with a scan rate of 100 mV/s. A Pt electrode was used as the working electrode versus a AgCl/Ag electrode as the reference electrode, and a Pt wire, as the counter electrode. The voltage was calibrated by using ferrocene as the internal standard.

Electrochemical Reductions. The reduction potentials of the OXD derivatives (10^{-3} M) were measured by cyclic voltammetry (CV) in dry tetrahydrofuran (THF) under N_2 with Bu_4NClO_4 (0.1 M) as the supporting electrolyte. The energy levels of the LUMO and HOMO were estimated according to their first half-reduction potentials[29] and optical band gaps (Table 2).

The first half-reduction potentials ($E_{1/2}^{red}$) of **1−10** fall into a wide range of −0.76 to −1.80 V (hereafter, all potential scales are versus AgCl/Ag) (Figure 10). These results imply that the substituent electronic effects on the LUMO of multi-(1,3,4-oxadiazo-2-yl)benzenes are strong.

The first $E_{1/2}^{red}$ of bisoxadiazoles **1−3** appears within a range of −1.52 to −1.80 V, which is much higher than that of −2.11 V for DPO. Although the $E_{1/2}^{red}$ of −1.80 V for the meta-OXD-substituted **3** is the lowest one due to weak electronic coupling, the $E_{1/2}^{red}$ of −1.52 V for **2** is much higher due to the strong π-conjugation between the para-OXD substituents; π-resonance stabilization of the radical anion $\mathbf{2}^-$ would effectively facilitate the electrochemical reduction process (Scheme 3). It is worth pointing out that **1** shows an unexpectedly high $E_{1/2}^{red}$ of −1.54 V, which is close to that of **2**, implying that $\mathbf{1}^-$ is also highly stabilized by the ortho-OXD units. This could be explained, provided that $\mathbf{1}^-$ is also planarized to keep the π-conjugation effective. This result is consistent with our previous conclusion in which a flattened geometry is presumed for the excited state of **1** when an electron is promoted by photoexcitation from the HOMO into the LUMO, which drives **1** into a fully coplanar geometry.

Electrochemical reduction becomes favorable when more electron-withdrawing OXD groups are introduced. Therefore, the $E_{1/2}^{red}$ of the trisubstituted **4−6** are generally higher, ranging from −1.34 to −1.65 V. This could be clearly observed when we compare the $E_{1/2}^{red}$ of **3** and **6**, in which the $E_{1/2}^{red}$ of −1.58 V for the 1,3,5-trisubstituted **6** is higher than the $E_{1/2}^{red}$ of −1.80 V

SCHEME 3: Anions of 1−3

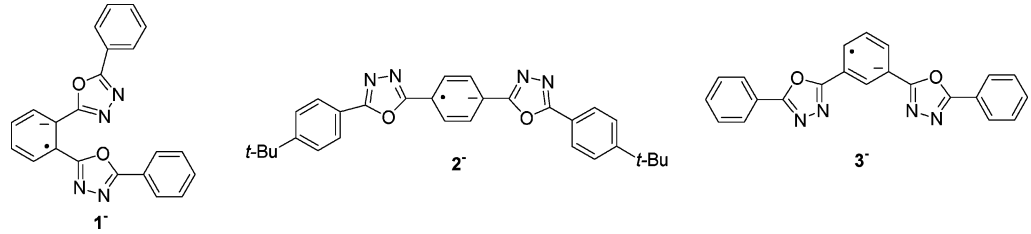

for the 1,3-disubstituted **3**. The $E_{1/2}^{red}$ of −1.65 V for the 1,2,3-substituted **4** is higher than that of **3**, but is lower than the 1,2-disubstituted **1**, which might be explained by the large steric hindrance in **4** that retards the conjugative stabilization. On the other hand, the $E_{1/2}^{red}$ of −1.34 V for the 1,2,4-substituted **5** is higher than that of **4** and **6**, which is due to the existence of the para-conjugations. As expected, tetra-, penta-, and hexa-substituted OXD derivatives have more electron-withdrawing substituents on the central ring and therefore would have higher $E_{1/2}^{red}$ than the others. Correlation plots of the number of the OXD units against the estimated LUMO energy levels are shown in Figure 11. The data could be unequivocally divided into two sets of clean-cut linear relationships. The upper line (red) consists of DPO, **3**, **4**, **6**, **8**, **9**, and **10** that would be classified as a nonconjugative group. All of their OXD groups are either meta-conjugated or highly ortho-substituted so that any coplanar alignments are prohibited. In these situations, the descending order of the LUMO energy level is correlated only to the number of the electron-withdrawing OXD units. The lower one (blue) consists of **1**, **2**, **5**, and **7** that belong to the conjugative class; their LUMO energy levels are not only dependent on the number of OXD units, but also governed by the conjugation between ortho/para OXD units. The $E_{1/2}^{red}$ of −0.76 V for **10** is superiorly high. By tuning the number and the positions of the OXD substituents, a wide range of reduction potentials ranging from an $E_{1/2}^{red}$ of −2.11 V for DPO to −0.76 V for **10** could be successfully achieved.

Photoluminescence Behaviors of 1−10 in a PVK Matrix. It has been reported that doping of the electron-deficient OXD compounds in an electron-rich arylamine-based matrix would allow formation of exciplexes under photoexcitation or electroluminescence.[30] Recently, other theories about the electroplex formation have also been discussed.[31] To determine whether exciplex or electroplex could be effectively generated in a physical blend of OXDs **1**−**10** in PVK, we first evaluated the the PL behaviors of **1**−**10** in PVK. Figure 12 shows the PL spectra of the PVK−OXD (*w*/*w* = 10:4) blend. Since the PVK−PBD blend is a common host matrix for PLED, we adopt this system as our reference for comparison. The PVK−PBD blend emits at 420 nm, which is slightly red-shifted in comparison to the emission of either pure PBD or PVK. The red-shifted photoluminescence of the PVK−PBD blend had been attributed to the exciplex emission.[6a,8f,g,18d,32]

Other PVK−OXD blends show emission at much more red-shifted regions, spanning a wide spectral range from blue (416 nm) to red (603 nm). Unlike the emissions in solution, all emissions from the PVK−OXD blends are broad and featureless. Although the red-shift phenomena could be explained by the exciplex theory, formation of ground-state charge-transfer (CT) complexes in the matrix might also be possible. To differentiate these two types of species, we selected **5** as a model to study. The absorption spectra of **5**, PVK, and the PVK−**5** blend are shown in Figure 13 for comparison. No new feature is observed when comparing the absorption spectrum of PVK−**5** blend against the individual spectra of **5** and PVK. On the other hand, the emission spectrum of the PVK−-**5** blend is more red-shifted than that of PVK or **5**. In addition, the excitation spectrum of the PVK−**5** blend, monitored at 517 nm, is more or less identical to the absorption spectrum, indicating that the possibility of the ground-state CT complex formation is invalid. Furthermore, correlations between the PL of the PVK−OXD blends versus the PL of the OXDs, either in solution or in solid film, are poor, again indicating that the emissions of the PVK−OXDs are not originating from the locally excited OXD. Since the red-shifted emission is originating not from PVK, not from **5**, and not from their excimers, we attribute this to the PVK−OXD exciplex emission.

To gain more insight into the photophysical behavior of the PVK−**5** blend, we then conducted pico- to nanosecond time-

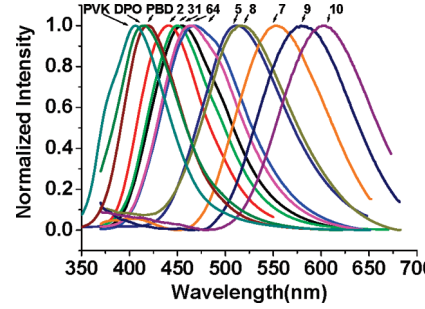

Figure 12. PL spectra of PVK−OXD blends.

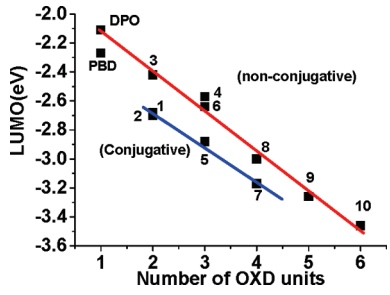

Figure 11. Correlation analyses of the LUMO energy level versus the number of OXD units on the central benzene ring.

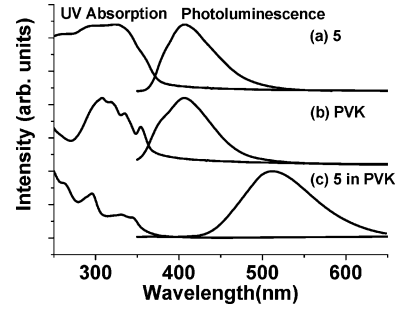

Figure 13. UV−vis spectra and photoluminescent spectra of (a) **5**, (b) PVK, and (c) PVK−**5** blend.

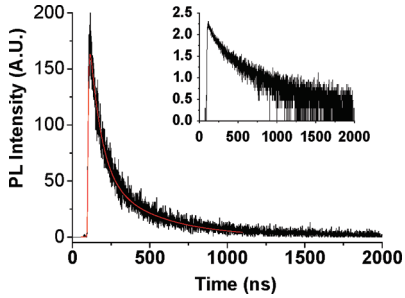

Figure 14. (Black) A typical decay curve for the PVK−**5** blend system monitored at 620 nm. Excitation wavelength: 365 nm. (Red) The fitting curve based on two single-exponential decay components ($\tau_1 \sim 70.04$ ns, $\tau_2 \sim 367.6$ ns, $\chi = 1.01$). Inset: The plot of the logarithm of emission intensity (signal counts) as a function of time.

TABLE 3: The Physical Properties of Blend Film and Neat Film

compound	emission lifetime[a,b]		QY × 10^2
PVK−**5**	τ_1: 70.04 (70%)	τ_2: 367.60 (30%)	0.1
PVK−**10**	τ_1: 4.37 (79%)	τ_2: 78.27 (21%)	0.05
PVK	τ_1: 2.61 (69%)	τ_2: 19.17 (31%)	
5	τ_1: 1.56		
10	τ_1: 1.1		

[a] Excitation λ/emission λ (nm) for PVK−**5**, 365/620; PVK−**10**, 375/670; PVK, 350/400; **5**, 365/400; **10**, 365/420; see Figures 2 and 12 for spectra. [b] Unit: ns; data in parentheses represents the pre-exponential factor, i.e., the contribution of the decay component at $t = 0$.

correlated, single-photon counting measurements (see the Experimental section for details). As for the control experiment, we also carried out the time-resolved measurement for the as-prepared PVK and compound **5**, respectively, in their neat film form. Figure 14 depicts a prototype of emission (monitored at 620 nm) relaxation dynamics for the PVK−**5** blend film (*w*/*w* = 10:4); pertinent kinetic data for PVK−**5** blend film, PVK, and **5** in neat solid film are listed in Table 3. Compound **5** in solid film reveals single-exponential decay kinetics with a lifetime of as short as 1.56 ns, and the PVK film exhibits multiexponential decay dynamics. To simplify the approach, the experimental results are fitted with a two-single-exponential decay protocol, and two decay components with lifetime of 2.6 and 19.2 ns are then deduced ($\chi = 1.05$). The result, to a certain extent, indicates the existence of heterostructures for the as-prepared PVK film. Similar multiexponential-like decay dynamics are observed for the PVK−**5** blend film (see inset of Figure 14 for the nonlinearity). The data nevertheless are well-fitted by two single-exponential decay components, rendering lifetimes of $\tau_1 \sim 70.04$ ns and $\tau_2 \sim 367.6$ ns ($\chi = 1.01$), which are remarkably longer than that of both compound **5** (1.56 ns) and PVK (<20 ns) in the neat film. This result, together with the drastically different emission spectral profile and peak wavelength (c.f. **5** and PVK, vide supra) and near independence of the solvent polarity, unambiguously supports the exciplex type of emission. Note that the lifetime of several tens to a few hundred nanoseconds for the exciplex emission are comparable to other exciplex systems, such as TFMO/PyPySPyPy blend films cast from para-xylene (PX) and chlorobenzene (CB) (~40−90 ns) reported by Nelso et al..[33] As shown in Figure 14, the rise time of the PVK−**5** emission is beyond the system response limit of 200 ps, indicating a perhaps ultrafast time scale of the exciplex formation. Similar long-lived exciplex emission is resolved for the PVK−**10** blend film (see Figure 12 and Table 3). Due to the possible heterogeneous environment of PVK that complicates the dynamic processes, detailed femotosecond dynamic studies to shed light on the mechanism of exciplex formation is not further pursued.

Last but not least, the quantum yields of exciplex emission for both PVK−**5** and PVK−**10** are low (see Table 3). This can be rationalized by the fact that the exciplex emission, having a transition to the repulsive potential energy surface of the ground state, is considered to be a forbidden process and is normally dominated by radiationless deactivation.

Electroluminescence Behaviors of 1−10 in PVK Matrix. The exciplexes emission could also be generated by EL. In our studies, PLED devices of indium tin oxide (ITO)/poly(3,4-ethylenedioxythiophene)-poly(styrenesulfonate)(PEDOT)−PSS/PVK−OXD/Mg−Ag were fabricated. The EL performances of the PVK−OXD blends are summarized in Table 3. Their normalized EL spectra are shown in Figure 15 for comparison. Similar to their PL spectra, their EL spectra spread over a wide range of the visible region, from 416 to 603 nm. A linear correlation between the λ_{max} of the EL and PL is observed (Figure 15b), implying that their emission mechanisms are similar. Little deviations between the EL and PL within a range of 7−34 nm with small fwhm differences from 1 to 25 nm are observed, suggesting that the EL and PL are originating from the same excited species. The small deviations between the EL and PL might be due to the device interference phenomenon.[34]

Generally speaking, in OLEDs, characteristic featureless and broad emission from exciplexes would occur at the solid interface between the HTL and ETL or from their homogeneous blend. The HTL acts as electron donors, and the ETL acts as electron acceptors. The emissions are usually red-shifted in comparison to the emissions either from the HTL or from the ETL. The contact electron−hole pair corresponds to a charge-transfer (CT) configuration, denoted as $|A^-D^+\rangle$, contributing to part of the electronic structure of the exciplex $\Psi_{ex} = C_1|A^*D\rangle + C_2|A^-D^+\rangle$, in which $|A^*D\rangle$ represents a locally excited configuration (LOC). The coefficients C_1 and C_2 determine the

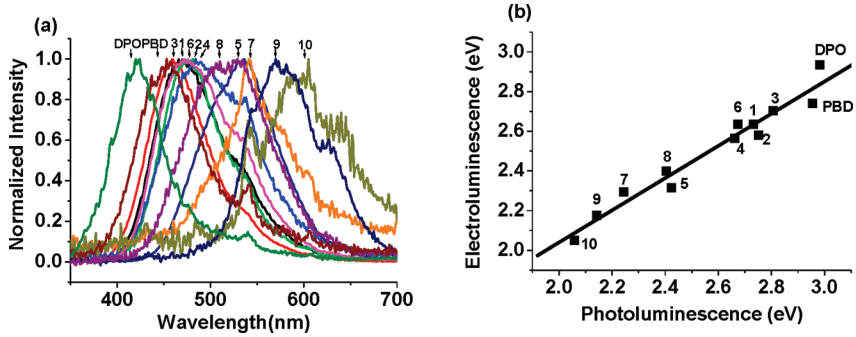

Figure 15. (a) EL spectra of PVK−OXD blends obtained at 12−14 V forward bias and (b) correlation plot of the λ_{max} of the EL and PL.

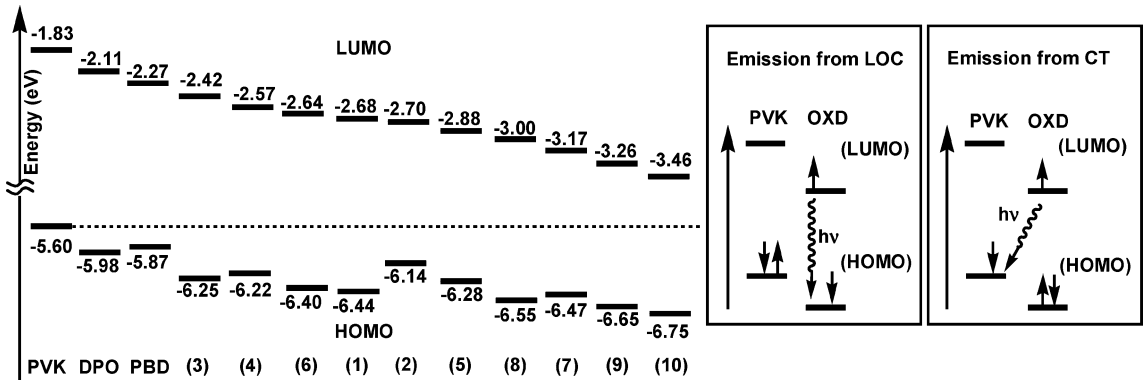

Figure 16. The HOMO−LUMO alignment diagram for PVK and OXD derivatives.

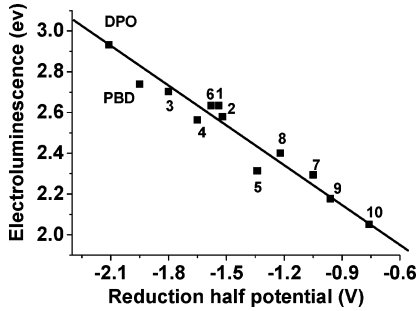

Figure 17. Correlation analysis for the reduction potential versus EL (eV).

extents of mixing between the LOC and CT configurations. The coefficient C_1 should be large in the local excited state, whereas the coefficient C_2 should be significant in the CT excited state. As the HOMO−LUMO alignment diagram illustrates in Figure 16, when the HOMO (donor)−HOMO (acceptor) gap and LUMO (donor)−LUMO (acceptor) gap are large, the possibility of having the electron back-flowed from acceptor (OXD) in the CT state to the donor (PVK) is low. In that situation, direct emission from the CT state would become predominant, and the emission from the LOC of the OXD can be ignored.

However, the theory of electroplex emission has recently been established. In this theory, formation of a charge-transfer complex in the EL mechanism has been suggested. Recently, the observations of EL from either molecular exciplexes or electroplexes have been frequently reported.[8a,10] The electroluminescent phenomena from the exciplexes[8] and electroplexes[10] were commonly observed in a mixed layer of electron-donating and -accepting molecules. However, emission through these mechanisms was usually weak with poor efficiency.[9] In our cases, the EL efficiency of **5** could be as high as 1.0 cd/A, which is unexpected. A plot of the EL emission energy versus the first $E_{1/2}^{red}$ of multi-(1,3,4-oxadiazo-2-yl)-substituted benzene derivatives shows a good linear correlation (Figure 17). This could clearly be explained by the classical exciplex theory. Although the electroplex theory could not be excluded, simultaneous observation of the almost identical PL and EL spectra supports the exciplex emission mechanism. Maximum exciplex emission ($h\nu^{max}$) of a family of derivatives can be expressed as $IP_D - EA_A + C$, where $h\nu^{max}$ refers to either an emission maximum, IP_D is the ionization potential of the donor, EA_A is the electron affinity of the acceptor, and C is the Coulombic attraction between the ion pair of D^+ and A^-. Thus, for using PVK as a common donor in our cases, the term of IP_D is constant and $h\nu^{max}$ will be proportional to EA_A, which is reflected in the reduction half-potentials.

Fabrication of the Near White Light EL Devices. Due to their interesting photophysical behaviors of exciplex emission, white organic light-emitting diodes based on exciplex electroluminescence has recently be explored.[35] Along with this line, herein, we have devised a new approach for near-white-light EL devices. It has been reported that the EL wavelength could be tuned by doping fluorescent dyes, such as coumarin 47, coumarin 6, and Nile red, into the PVK−PBD matrix.[6] Therefore, a blue light EL device could also be fabricated by this approach using a blue light fluorescent emitter. As we described before, PVK−**5** shows highly efficient yellow EL. We wonder if PVK−**5** could be used as a yellow emitter for white light PLEDs. Since PVK−**5** has a large Stokes shift with no absorption in the blue region (Figure 13), quenching of the blue emission from the dye through energy transfer to PVK−**5** could therefore be avoided. In this situation, we expect to see blue-yellow duo emissions from the device of PVK−PBD−blue dye emitter−**5**.

In our attempt, we adopted 2,5,8,11-tetra-*tert*-butylperylene (TBPe) as a blue fluorescent dopant. The PVK−PBD−TBPe device emits blue light at 460 nm with a shoulder band at 486 nm (Figure 18a, line b). The current efficiency of 1.22 cd/A with a brightness of 300 cd/m^2 was achieved (Table 4). Figure 18a shows the EL spectrum of the device of PVK−PBD−TBPe−**5** (line a), which is composed of the emission bands from TBPe (line b) as well as the exciplex of PVK−**5** (line c). The unbalanced emission intensities of the yellowish band over the blue band suggest that the emission process from PVK−**5** is much more efficient than that of TBPe. The relative intensity of the blue emission could be enhanced (Figure 18b) by either increasing the weight of TBPe (Table 4, entry 3) or increasing the weight of PBD (Table 4, entry 4). These results suggest that the emission band is tunable by adjusting the dopant compositions. Among the devices we tried, the device of PVK−PBD−**5**−TBPe (100 mg:40 mg:40 mg:4 mg) gave the highest brightness with good current efficiency of 1.63 cd/A.

Conclusion

In summary, our results provide solid evidence to support the exciplex emission phenomena in the organic electroluminescence of PVK−OXD blends. Although one might suspect that substantial charge transfer in the excited state would become predominant by tuning down the LUMO of the OXDs so that formation of the electroplex could be facilitated, our results indicated that the exciplex formation is still predominant; even the LUMO level of the OXD spans a wide range from −2.11 to −3.46 eV. The linear correlation between the $E_{1/2}^{red}$ and the λ_{max} of EL (eV) reflected that the term of the charge transfer (CT) configuration of the contact electron−hole pair, denoted

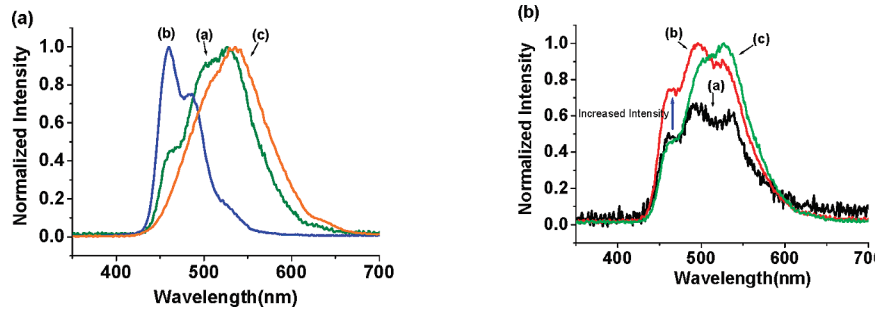

Figure 18. (a) Electroluminescence spectra of (line a) PVK−PBD−**5**−TBPe blend (100 mg:40 mg:40 mg:2 mg). (line b) PVK−PBD−TBPe blend (100 mg:40 mg:2 mg). (line c) PVK−**5** blend (100 mg:40 mg). (b) Electroluminescence spectra of (line a) PVK−PBD−**5**−TBPe blend (100 mg:60 mg:40 mg:2 mg). (line b) PVK−PBD−**5**−TBPe blend (100 mg:40 mg:40 mg:4 mg). (line c) PVK−PBD−**5**−TBPe blend (100 mg:40 mg:40 mg:2 mg).

TABLE 4: EL Performance of the PVK-OXD Blending Layers[e]

OXD	V_{on}[a], V	LE_{max}[b], cd/A	B_{max}[c], cd/m^2	$V_{B,max}$[d], V	λ (EL) (fwhm), nm	CIE1931, (x, y)	υ (PL) (fwhm), nm
1	6.9	0.32	62	14	471 (94)	(0.170, 0.251)	454 (89)
2	7.3	0.42	106	14	481 (80)	(0.172, 0.264)	442 (76)
3	7.5	0.24	65	12	459 (75)	(0.161, 0.172)	451 (83)
4	7.2	0.48	58	13	484 (112)	(0.215, 0.352)	466 (98)
5	4.4	1.02	267	12	536 (97)	(0.291, 0.529)	512 (101)
6	8.0	0.14	58	13	471 (109)	(0.187, 0.288)	464 (93)
7	10.1	0.03	8	16	541 (82)	(0.357, 0.491)	553 (107)
8	9.2	0.06	14	13	517 (108)	(0.255, 0.466)	516 (104)
9	6.2	0.34	73	14	570 (103)	(0.473, 0.495)	579 (109)
10	7.5	0.04	15	13	605 (116)	(0.476, 0.432)	603 (109)
PBD	9.1	0.31	49	16	453 (80)	(0.195, 0.187)	420 (69)
DPO	10.5	0.02	13	15	423 (63)	(0.178, 0.114)	416 (78)

[a] Turn-on voltage at 1 cd/m^2. [b] Maximum luminescence current efficiency. [c] Maximum brightness. [d] Voltage at maximum brightness. [e] ITO/PEDOT/PSS (50 nm)/PVK/OXD (70 nm)/Mg (2 nm)/Ag (1000 nm).

TABLE 5: Performance of Dye-Doped EL Devices[e]

devices (wt ratio)	V_{on}, V[a]	LE_{max}, cd/A[b]	B_{max}, cd/m^2[c]	$V_{B,max}$, V[d]	CIE1931, (x, y)
PVK−PBD−TBPe (100 mg:40 mg:2 mg)	8.2	1.22	306	14	(0.137, 0.157)
PVK−PBD−**5**−TBPe (100 mg:40 mg:40 mg:2 mg)	8.1	1.65	434	17	(0.230, 0.483)
PVK−PBD−**5**−TBPe (100 mg:40 mg:40 mg:4 mg)	5.7	1.63	596	16	(0.210, 0.405)
PVK−PBD−**5**−TBPe (100 mg:60 mg:40 mg:2 mg)	8.1	1.16	256	18	(0.246, 0.402)

[a] Turn-on voltage at 1 cd/m^2. [b] Maximum luminescence current efficiency. [c] Maximum brightness. [d] Voltage at maximum brightness. [e] The film thickness of light emitting layer was 110 nm.

as $|A^-D^+\rangle$ in $\Psi_{ex} = C_1|A^*D\rangle + C_2|A^-D^+\rangle$, would have a major contribution to the exciplex emission. In our cases, the EL efficiency of **5** could be as high as 1.0 cd/A. Since the exciplex emission usually has a large Stokes shift, this provides a window for us to design duo emissions for near-white-light EL with high efficiency. Among the devices we tried, the device of PVK−PBD−**5**−TBPe (100 mg:40 mg:40 mg:4 mg) gave EL with a good current efficiency of 1.63 cd/A.

Experimental Section

General Procedures. All reagents and solvents were of analytical or chemical grade and purified using standard methods. Electrochemical reduction behavior of the compounds was measured by CV (scan rate = 100 mV/s) in THF using Bu_4NClO_4 (0.1 M) as the supporting electrolyte with a Pt electrode as the working electrode and a Pt wire as the counter electrode and a Ag/AgCl, KCl (saturated) electrode as the reference electrode. The emission quantum yield for all OXDs was measured in THF against coumarin 1 (quantum yield: 0.85) as standard.[36]

Steady-state absorption and emission spectra were recorded by a Hitachi (U-3310) spectrophotometer and an Edinburgh (FS920) fluorometer, respectively. UV−vis and fluorescence spectra were collected between 200 and 800 nm. Low-temperature fluorescence spectra were collected in 2-MeTHF at 77 K between 300 and 600 nm. For solution, the emission quantum yields were measured at excitation wavelength λ_{ex} = 350 nm at room temperature. In this approach, quinine sulfate with an emission yield of $\Phi \sim 0.54 \pm 0.2$ in 1.0 N sulfuric acid solution served as the standard to calculate the emission quantum yield. Front-face excitation was used to measure the emission of the solid film. A combination of appropriate filters was used to avoid interference from the scattering light. An integrating sphere was applied to measure the quantum yield in the solid film. The resulting luminescence was acquired by an intensified charge-coupled detector for subsequent quantum yield analyses. Lifetime studies were performed by an Edinburgh FL 900-L time-correlated single-photon counting system with a hydrogen-filled or a nitrogen lamp as the excitation source. Data were analyzed using a nonlinear least-squares procedure in combination with an iterative convolution method. Emission decays were analyzed by the sum of exponential functions, which allows partial removal of the instrument time broadening and consequently renders a temporal resolution of ~200 ps.

1,2-Bis[5-phenyl-(1,3,4)-oxadiazol-2-yl]benzene (1). (A general procedure for **1**−**3**.) 1,2-Bis(5-tetrazolyl)benzene (3.0 g, 14.0 mmol) and benzoyl chloride (7.9 g, 56.0 mmol) were dissolved in pyridine (35 mL). The solution was heated at 90

°C for 24 h. When the reaction was completed, the pyridine was removed under vacuum. The residue was digested with EtOH, and the product was precipitated from the solution. The product was filtered, collected, and washed with EtOH to give a white solid (3.0 g, 58%): mp 128−129 °C. ^{1}H NMR (400 MHz, $CDCl_3$, δ): 8.16−8.12 (m, 2H), 7.91−7.88 (m, 4H), 7.77−7.73 (m, 2H), 7.46−7.43 (m, 2H), 7.36 (t, J = 8 Hz, 4H). ^{13}C NMR (100 MHz, $CDCl_3$, δ): 165.2, 163.3, 131.9, 131.8, 130.8, 129.0, 126.9, 123.5, 123.3. MS (FAB) 367 (M^+ + H). HRMS (FAB) calcd for $C_{22}H_{15}N_4O_2$: 367.1195 (M^+ + H), obsd. 367.1198. Anal. Calcd for $C_{22}H_{14}N_4O_2$: C, 72.12; H, 3.85; N, 15.29. Found: C, 72.08; H, 3.63; N, 15.37.

1,4-Bis[5-(4-tert-butylphenyl)-(1,3,4)-oxadiazol-2-yl]benzene (2). 1,4-Bis(5-tetrazolyl)benzene (1.5 g, 7.0 mmol) and 4-*tert*-butylbenzoyl chloride (3.4 g, 17.5 mmol) were reacted to give product (2.9 g, 86%). mp 337−338 °C. ^{1}H NMR (400 MHz, $CDCl_3$, δ): 8.30 (s, 4H), 8.07 (d, J = 8 Hz, 4H), 7.55 (d, J = 8 Hz, 4H), 1.37 (s, 18H). ^{13}C NMR (100 MHz, $CDCl_3$, δ): 164.9, 163.3, 155.5, 127.3, 126.8, 126.5, 126.0, 120.7, 35.2, 31.2. MS (EI) 478 (M^+); HRMS (EI) calcd for $C_{30}H_{30}N_4O_2$ 478.2369 (M^+), obsd. 478.2366. Anal. Calcd for $C_{30}H_{30}N_4O_2$: C, 75.29; H, 6.32; N, 11.71. Found: C, 75.25; H, 6.30; N, 11.64.

4.2.3. 1,3-Bis[5-phenyl-(1,3,4)-oxadiazol-2-yl]benzene (3). 5-Phenyl-1*H*-tetrazole (1.5 g, 10.3 mmol) and isophthaloyl dichloride (1.0 g, 4.9 mmol) were reacted to give product (1.4 g, 80%). mp 146−147 °C. ^{1}H NMR (400 MHz, $CDCl_3$, δ): 8.84−8.83 (m, 1H), 8.33−8.30 (m, 2H), 8.18−8.14 (m, 4H), 7.71 (t, J = 8 Hz, 1H), 7.58−7.52 (m, 6H). ^{13}C NMR (100 MHz, $CDCl_3$, δ): 164.8, 163.4, 131.9, 129.9, 129.6, 129.0, 126.9, 124.9, 124.8, 123.4. HRMS (EI) calcd for $C_{22}H_{14}N_4O_2$: 366.1117 (M^+), obsd. 366.1111. Anal. Calcd for $C_{22}H_{14}N_4O_2$: C, 72.12; H, 3.85; N, 15.29. Found: C, 72.04; H, 3.84; N, 15.25.

1,2,3-Tri[5-phenyl-(1,3,4)-oxadiazol-2-yl]benzene (4). (A general procedure for **4, 5, 7**−**10**.) 1,2,3-Benzenetricarboxylic acid (1.0 g, 4.8 mmol) was digested with PCl_5 (5.0 g, 23.8 mmol) at 150 °C for 24 h. The excess PCl_5 was distilled off, and the residue was dissolved in benzene. The solution was transferred to another round-bottom flask and dried under vacuum to provide a crude acid chloride. The crude acid chloride and 5-phenyl-1*H*-tetrazole (3.5 g, 23.8 mmol) were dissolved in pyridine (3 mL). The solution was heated at 90 °C for 24 h. When the reaction was completed, the pyridine was removed by vacuum distillation. EtOH was added to precipitate the product. The product was filtered, collected, and washed with EtOH to give a crude solid that was purified by chromatography on silica gel using $Et_2O/CHCl_3$(1:5) as the eluent to give product (0.7 g, 30%). mp 250−251 °C. ^{1}H NMR (400 MHz, $CDCl_3$, δ): 8.61 (d, J = 8 Hz, 2H), 8.20−8.17 (m, 2H), 7.98 (t, J = 8 Hz, 1H), 7.83−7.81 (m, 4H), 7.58−7.54 (m, 3H), 7.45−7.41 (m, 2H), 7.32−7.28 (m, 4H). ^{13}C NMR (100 MHz, $CDCl_3$, δ): 165.7, 164.9, 161.9, 160.7, 132.4, 132.0, 131.4, 129.1, 128.9, 127.0, 126.8, 126.7, 123.5, 122.9. MS (EI) 510 (M^+). HRMS (EI) calcd for $C_{30}H_{18}N_6O_3$ 510.1440 (M^+), obsd. 510.1440. Anal. Calcd for $C_{30}H_{18}N_6O_3$: C, 70.58; H, 3.55; N, 16.46. Found: C, 70.22; H, 3.83; N, 16.32.

1,2,4-Tri[5-phenyl-(1,3,4)-oxadiazol-2-yl]benzene (5). 1,2,4-Benzenetricarboxylic anhydride (1.0 g, 5.2 mmol) was digested with PCl_5 (5.4 g, 26.0 mmol) to give crude acid chloride. The crude acid chloride and 5-phenyl-1*H*-tetrazole (3.8 g, 26.0 mmol) were reacted to give product (1.0 g, 38%). mp 243−244 °C. ^{1}H NMR (400 MHz, $CDCl_3$, δ): 8.84 (d, J = 2 Hz, 1H), 8.53 (dd, J = 8 Hz, J = 2 Hz, 1H), 8.34 (d, J = 8.4 Hz, 1H), 8.19−8.17 (m, 2H), 7.98−7.95 (m, 2H), 7.93−7.90 (m, 2H), 7.61−7.53 (m, 3H), 7.51−7.36 (m, 6H). ^{13}C NMR (100 MHz, $CDCl_3$, δ): 165.4, 165.3, 162.5, 162.3, 132.2, 132.0, 131.4, 129.5, 129.1, 128.99, 128.97, 128.88, 127.1, 127.0, 126.9, 126.8, 125.8, 124.4, 123.2, 123.0, 122.96. MS (EI) 510 (M^+). HRMS (EI) calcd for $C_{30}H_{18}N_6O_3$ 510.1440 (M^+), obsd. 510.1444. Anal. Calcd for $C_{30}H_{18}N_6O_3$: C, 70.58; H, 3.55; N, 16.46. Found: C, 70.54; H, 3.54; N, 16.86.

4.2.6. 1,2,4,5-Tetra[5-phenyl-(1,3,4)-oxadiazol-2-yl]benzene (7). Pyromellitic dianhydride (0.2 g, 0.5 mmol) and one drop of $POCl_3$ were digested with PCl_5 (0.4 g, 2.0 mmol) at 150 °C for 24 h. The crude acid chloride and 5-phenyl-1*H*-tetrazole (0.8 g, 5.5 mmol) were reacted to give product (0.3 g, 53%). mp 310−311 °C. ^{1}H NMR (400 MHz, $CDCl_3$, δ): 8.92 (s, 2H), 8.00−7.98 (m, 8H), 7.54−7.49 (m, 4H), 7.45−7.41 (m, 8H). ^{13}C NMR (100 MHz, $CDCl_3$, δ): 165.7, 161.3, 132.8, 132.2, 129.1, 127.0, 126.1, 122.8. MS (EI) 654 (M^+). HRMS (EI) calcd for $C_{38}H_{22}N_8O_4$ 654.1764 (M^+), obsd. 654.1766. Anal. Calcd for $C_{38}H_{22}N_8O_4$: C, 69.72; H, 3.39; N, 17.12. Found: C, 69.25; H, 3.62; N, 17.46.

1,2,3,5-Tetra[5-phenyl-(1,3,4)-oxadiazol-2-yl]benzene (8). 1,2,3,5-Benzenetetraicarboxylic acid (1.0 g, 3.9 mmol) was digested with PCl_5 (9.9 g, 47.3 mmol) to give crude acid chloride. The crude acid chloride and 5-phenyl-1*H*-tetrazole (4.6 g, 31.6 mmol) were reacted to give product (0.7 g, 28%). mp 353−354 °C. ^{1}H NMR(400 MHz, $CDCl_3$, δ): 9.31(s, 2H), 8.27−8.25 (m, 2H), 8.21−8.19 (m, 2H), 7.90−7.88 (m, 4H), 7.64−7.53 (m, 6H), 7.48 (t, J = 7.8 Hz, 2H), 7.35 (t, J = 8.0 Hz, 4H). ^{13}C NMR (100 MHz, D_2SO_4 as solvent with internal standard of $CDCl_3$): 167.7, 167.3, 166.6, 161.2, 160.1, 158.3, 140.2, 132.8, 130.9, 130.2, 125.7, 122.2, 121.3, 116.8, 114.2, 113.9, 113.8. MS (FAB) 655 (M^+ + H). HRMS (FAB) calcd for $C_{38}H_{23}N_8O_4$ 655.1842 (M^+ + H), obsd. 655.1848. Anal. Calcd for $C_{38}H_{22}N_8O_4$: C, 69.72; H, 3.39; N, 17.12. Found: C, 69.89; H, 3.76; N, 17.49.

1,2,3,4,5-Penta[5-phenyl-(1,3,4)-oxadiazol-2-yl]benzene (9). Benzenepentacarboxylic acid (2.0 g, 6.8 mmol) was digested with PCl_5 (16.8 g, 80.7 mmol) to give crude acid chloride. The crude acid chloride and 5-phenyl-1*H*-tetrazole (7.8 g, 53.0 mmol) were reacted to give product (0.1 g, 2%). mp 298−300 °C. ^{1}H NMR (400 MHz, $CDCl_3$, δ): 9.58 (s, 1H), 8.14 (dd, J = 7.6 Hz, 1.6 Hz, 4H), 7.90 (dd, J = 8.8 Hz, 1.2 Hz, 4H), 7.64 (dd, J = 8.8 Hz, 1.2 Hz, 2H), 7.61−7.57 (m, 2H), 7.54 (d, J = 7.6 Hz, 3H), 7.51−7.47 (m, 3H), 7.38−7.34 (m, 5H), 7.14 (t, J = 8.0 Hz, 2H). ^{13}C NMR (100 MHz, $CDCl_3$, δ): 166.0, 165.7, 165.3, 160.6, 159.4, 159.3, 132.5, 132.2, 130.7, 130.5, 129.6, 129.1, 129.0, 128.8, 127.15, 127.07, 126.9, 126.8, 125.6, 123.1, 122.4, 122.2. MS (FAB) 799 (M^+ + H). HRMS (FAB) calcd for $C_{46}H_{27}N_{10}O_5$ 799.2166 (M^+ + H), obsd. 799.2156. Anal. Calcd for $C_{46}H_{26}N_{10}O_5$: C, 69.17; H, 3.28; N, 17.54. Found: C, 69.08; H, 3.50; N, 18.10.

1,2,3,4,5,6-Hexa[5-phenyl-(1,3,4)-oxadiazol-2-yl]benzene (10). Mellitic acid (1.0 g, 3.0 mmol) was digested with PCl_5 to give crude acid chloride. The crude acid chloride and 5-phenyl-1*H*-tetrazole (4.3 g, 29.2 mmol) were reacted to give product (0.07 g, 3%). mp 304−305 °C. ^{1}H NMR (400 MHz, $CDCl_3$, δ): 7.85 (d, J = 7.2 Hz, 12H), 7.48 (t, J = 7.2 Hz, 6H), 7.34 (t, J = 8 Hz, 12H). ^{13}C NMR (100 MHz, $CDCl_3$, δ): 165.9, 158.7, 132.4, 130.2, 129.0, 127.0, 122.4. MS (FAB) 943 (M^+ + H). HRMS (FAB) calcd for $C_{54}H_{31}N_{12}O_6$ 943.2490 (M^+ + H), obsd. 943.2486. Anal. Calcd for $C_{54}H_{30}N_{12}O_6$: C, 68.79; H, 3.21; N, 17.83. Found: C, 68.92; H, 3.39; N, 17.97.

Benzene-1,3,5-tricarboxylic Acid Trimethyl Ester. A solution of benzene-1,3,5-tricarboxyl acid (5.0 g, 23.8 mmol) in MeOH (47 mL) and H_2SO_4 (98%, 5 mL) was heated at 80 °C for 24 h. When the reaction was completed, most of the MeOH was

removed by rotary evaporation under vacuum, and the crude product was extracted with $CHCl_3$ and water. The organic layer was dried over anhydrous Na_2SO_4 and concentrated under vacuum to give a white solid (5.7 g, 96%). mp 255−256 °C. ^{1}H NMR (400 MHz, $CDCl_3$, δ): 8.84 (s, 3H), 3.97 (s, 9H). ^{13}C NMR (100 MHz, $CDCl_3$, δ): 165.1, 134.4, 131.0, 52.7. MS (EI) 252 (M^+). HRMS (EI) calcd for $C_{12}H_{12}O_6$ 252.0634 (M^+), obsd. 252.0633. Anal. Calcd for $C_{12}H_{12}O_6$: C, 57.14; H, 4.80. Found: C, 57.04; H, 4.57.

Reaction Sequence for the Preparation of 1,3,5-Tri[5-phenyl-(1,3,4)-oxadiazol-2-yl]benzene (6). ***Benzene-1,3,5-tricarboxylic Acid Trihydrazide.*** To a solution of benzene-1,3,5-tricarboxylic acid trimethyl ester (5.0 g, 19.8 mmol) in EtOH (30 mL) and toluene (30 mL) under nitrogen atmosphere was added hydrazine hydrate (14.5 mL, 297.0 mmol). The solution was heated at 110 °C for 24 h, and the crude product was precipitated during reaction. The product was collected by filtration and washed with EtOH and toluene to give a white solid (4.6 g, 92%). mp >400 °C. ^{1}H NMR (400 MHz, DMSO-d_6, δ): 9.83 (s, 3H), 8.30 (s, 3H), 4.57 (br, 6H). ^{13}C NMR (100 MHz, DMSO-d_6, δ): 164.7, 133.6, 127.9. MS (EI) 252 (M^+). HRMS (EI) calcd for $C_9H_{12}N_6O_3$ 252.0971 (M^+), obsd. 252.0976. Anal. Calcd for $C_9H_{12}N_6O_3$: C, 42.86; H, 4.80; N, 33.32. Found: C, 42.62; H, 4.74; N, 33.22.

N′,N‴,N⁗′-Tri(benzoyl)benzene-1,3,5-tricarboxylic Acid Trihydrazide. A solution of benzene-1,3,5-tricarboxylic acid trihydrazide (1.0 g, 4.0 mmol) in dry NMP (10 mL) at 0 °C was kept for 20 min. Benzoyl chloride (1.4 mL, 12.3 mmol) was added into the solution, and the solution was allowed to stand overnight. The solution was added dropwise into water, and a white solid was precipitated. The white crude product was collected by filtration and washed with hot EtOH to give a white solid (2.2 g, 99%). mp 279−295 °C. ^{1}H NMR (400 MHz, DMSO-d_6, δ): 10.85 (s, 3H), 10.65 (s, 3H), 8.64 (s, 3H), 7.94 (d, J = 7.2 Hz, 6H), 7.63−7.51 (m, 9H). ^{13}C NMR (100 MHz, DMSO-d_6, δ): 165.5, 164.7, 133.3, 132.2, 131.8, 129.6, 128.4, 127.3. MS (FAB) 565 (M^+ + H). HRMS (FAB) calcd for $C_{30}H_{25}N_6O_6$ 565.1836 (M^+ + H), obsd. 565.1823. Anal. Calcd for $C_{30}H_{24}N_6O_6$: C, 75.29; H, 6.32; N, 11.71 Found: C, 75.29; H, 6.32; N, 11.85.

1,3,5-Tri[5-phenyl-(1,3,4)-oxadiazol-2-yl]benzene(6). *N′,N‴,N⁗′*-Tri(benzoyl)benzene-1,3,5-tricarboxylic acid trihydrazide (1.5 g, 2.7 mmol) was dissolved in $POCl_3$ (27 mL). The solution was heated at 105 °C overnight. The solution was added dropwise into ice water, and a brown solid precipitated. The crude product was collected by filtration and washed with $NaHCO_{3(aq)}$. The solid was purified by chromatography on silica gel using $Et_2O/CHCl_3$(1:5) as the eluent to give product (1.2 g, 91%). mp 350−351 °C. ^{1}H NMR (400 MHz, $CDCl_3$, δ): 9.07 (s, 3H), 8.24−8.22 (m, 6H), 7.62−7.57 (m, 9H). ^{13}C NMR (100 MHz, $CDCl_3$, δ): 165.3, 162.6, 132.2, 129.1, 127.19, 127.15, 126.2, 123.2. MS (EI) 510 (M^+). HRMS (EI) calcd for $C_{30}H_{18}N_6O_3$ 510.1440 (M^+), obsd. 510.1433. Anal. Calcd for $C_{30}H_{18}N_6O_3$: C, 70.58; H, 3.55; N, 16.46. Found: C, 70.12; H, 3.58; N, 16.42.

Acknowledgment. The present work was supported by the Ministry of Eduction and National Taiwan University, National Science Council of Taiwan (NSC-95-2113-M002-021-MY3, NSC-98-2119-M-002-006-MY3, and NSC-97-3114-M-002-005), and Academia Sinica (Thematic Project).

Supporting Information Available: ^{1}H and ^{13}C NMR spectra and their preparation procedures and UV-vis and fluorescence spectra (pdf, 42 pages). This material is available free of charge via the Internet at http://pubs.acs.org.

References and Notes

(1) Tang, C. W.; VanSlyke, S. A. *Appl. Phys. Lett.* **1987**, *51*, 913.

(2) (a) Tamoto, N.; Adachi, C.; Nagai, K. *Chem. Mater.* **1997**, *9*, 1077. (b) Baldo, M. A.; O'Brien, D. F.; You, Y.; Shoustikov, A.; Sibley, S.; Thompson, M. E.; Forrest, S. R. *Nature* **1998**, *395*, 151.

(3) (a) Burroughes, J. H.; Bradley, D. D. C.; Brown, A. R.; Marks, R. N.; Mackay, K.; Friend, R. H.; Burn, P. L.; Holmes, A. B. *Nature* **1990**, *347*, 539. (b) Parker, I. D.; Cao, Y.; Yang, C. Y. *J. Appl. Phys.* **1999**, *85*, 2441. (c) Cao, Y.; Parker, I. D.; Yu, G.; Zhang, C.; Heeger, A. J. *Nature* **1999**, *397*, 414. (d) Ho, P. K. H.; Kim, J. S.; Burroughes, J. H.; Becker, H.; Li, S. F. Y.; Brown, T. M.; Cacialli, F.; Friend, R. H. *Nature* **2000**, *404*, 481. (e) Gross, M.; Muller, D. C.; Nothofer, H. G.; Scherf, U.; Neher, D.; Brauchle, C.; Meerholz, K. *Nature* **2000**, *405*, 661.

(4) (a) Kido, J.; Kimura, M.; Nagai, K. *Science* **1995**, *267*, 1332. (b) Tasch, S.; List, E. J. W.; Ekström, O.; Graupner, W.; Leising, G.; Schlichting, P.; Rohr, U.; Geerts, Y.; Scherf, U.; Müllen, K. *Appl. Phys. Lett.* **1997**, *71*, 2883.

(5) Kido, J.; Hongawa, K.; Okuyama, K.; Nagai, K. *Appl. Phys. Lett.* **1993**, *63*, 2627.

(6) (a) Kido, J.; Shionoya, H.; Nagai, K. *Appl. Phys. Lett.* **1995**, *67*, 2281. (b) Wu, C. C.; Sturm, J. C.; Register, R. A.; Tian, J.; Dana, E. P.; Thompson, M. E. *IEEE Trans. Electron Devices* **1997**, *44*, 1269.

(7) (a) Peng, Z.; Bao, Z.; Galvin, M. E. *Adv. Mater.* **1998**, *10*, 680. (b) Jiang, X.; Register, R. A.; Killeen, K. A.; Thompson, M. E.; Pschenitzka, F.; Sturm, J. C. *Chem. Mater.* **2000**, *12*, 2542.

(8) (a) Osaheni, J. A.; Jenekhe, S. A. *Macromolecules* **1994**, *27*, 739. (b) Gebler, D. D.; Wang, Y. Z.; Fu, D.-K.; Swager, T. M.; Epstein, A. J. *J. Chem. Phys.* **1998**, *108*, 7842. (c) Wang, Y. Z.; Gebler, D. D.; Spry, D. J.; Fu, D. K.; Swager, T. M.; MacDiarmid, A. G.; Epstein, A. J. *IEEE Trans. Electron Devices* **1997**, *44*, 1263. (d) Hu, B.; Yang, Z.; Karasz, F. E. *J. Appl. Phys.* **1994**, *76*, 2419. (e) Wang, J. F. *Adv. Mater.* **1998**, *10*, 230. (f) Thompson, J.; Blyth, R. I. R.; Mazzeo, M.; Anni, M.; Gigli, G.; Cingolani, R. *Appl. Phys. Lett.* **2001**, *79*, 560. (g) Jiang, X.; Register, R. A.; Killen, K. A.; Thompson, M. E.; Pschenitzka, F.; Hebner, T. R.; Sturm, J. C. *J. Appl. Phys.* **2002**, *91*, 6717. (i) Zhao, D.; Zhang, F.; Xu, C.; Sun, J.; Song, S.; Xu, Z.; Sun, X. *Appl. Surf. Sci.* **2008**, *254*, 3548. (j) Castellani, M.; Berner, D. *J. Appl. Phys.* **2007**, *102*, 024509. (k) Wang, D.; Li, W.; Chu, B.; Su, Z.; Bi, D.; Zhang, D.; Zhu, J.; Yan, F.; Chen, Y.; Tsuboi, T. *Appl. Phys. Lett.* **2008**, *92*, 053304. (l) Yang, J.; Gordon, K. C. *Chem. Phys. Lett.* **2003**, *375*, 649.

(9) (a) Adachi, C.; Tsutsui, T.; Saito, S. *Appl. Phys. Lett.* **1990**, *56*, 799. (b) Yamamoto, T.; Inoue, T.; Kanbara, T. *Jpn. J. Appl. Phys., Part 2* **1994**, *33*, L250. (c) Gebler, D. D.; Wang, Y. Z.; Blatchford, J. W.; Jessen, S. W.; Fu, D.-K.; Swager, T. M.; MacDiarmid, A. G.; Epstein, A. J. *Appl. Phys. Lett.* **1997**, 7–1644. (e) Yang, Y.; Pei, Q. *Appl. Phys. Lett.* **1997**, *70*, 1926. (f) Jenekhe, S. A.; Osaheni, J. A. *Science* **1994**, *265*, 765. (g) Jenekhe, S. A. *Adv. Mater.* **1995**, *7*, 309. (h) Morteani, A. C.; Friend, R. H.; Silva, C. *J. Chem. Phys.* **2005**, *122*, 244906. *Chem. Phys. Lett.* **2004**, *391*, 81. (i) Morteani, A. C.; Dhoot, A. S.; Kim, J.-s.; Silva, C.; Greenham, N. C.; Murphy, C.; Moons, E.; Cina, S.; Burroughes, J. H.; Friend, R. H. *Adv. Mater.* **2003**, *15*, 1708.

(10) (a) Granlund, T.; Pettersson, L. A. A.; Anderson, M. R.; Inganäs, O. *J. Appl. Phys.* **1997**, *81*, 8097. (b) Giro, G.; Cocchi, M.; Kalinowski, J.; Di Marco, P.; Fattori, V. *Chem. Phys. Lett.* **2000**, *318*, 137. (c) Kalinowski, J.; Cocchi, M.; Di Marco, P.; Stampor, W.; Giro, G.; Fattori, V. *J. Phys. D: Appl. Phys.* **2000**, *33*, 2379. (d) Wang, Y.; Teng, F.; Xu, Z.; Hou, Y.; Wang, Y.; Xu, X. *Eur. Polym. J.* **2005**, *41*, 1020. (e) Kalinowski, J.; Giro, G.; Cocchi, M.; Fattori, V.; Di Marco, P. *Appl. Phys. Lett.* **2000**, *76*, 2352. (f) Zhao, D.-W.; Xu, Z.; Zhang, F.-J.; Song, S.-F.; Zhao, S.-L.; Wang, Y.; Yuan, G.-C.; Zhang, Y.-F.; Xu, H.-H. *Appl. Surf. Sci.* **2007**, *253*, 4025. For recent discussions about exciplex formation and charge separation, see (g) Petrova, M. V.; Burshtein, A. I. *J. Phys. Chem. A* **2008**, *112*, 13343. **2009**, *113*, 2405. (h) Benson-Smith, J. J.; Wilson, J.; Dyer-Smith, C.; Mouri, K.; Yamaguchi, S.; Murata, H.; Nelson, J. *J. Phys. Chem. B* **2009**, *113*, 7794.

(11) (a) Hughes, G.; Bryce, M. R. *J. Mater. Chem.* **2005**, *15*, 94. (b) Kulkarni, A. P.; Tonzola, C. J.; Babel, A.; Jenekhe, S. A. *Chem. Mater.* **2004**, *16*, 4556.

(12) (a) Wang, C.; Jung, G.-Y.; Hua, Y.; Pearson, C.; Bryce, M. R.; Petty, M. C.; Batsanov, A. S.; Goeta, A. E.; Howard, J. A. K. *Chem. Mater.* **2001**, *13*, 1167. (b) Wang, C.; Jung, G.-Y.; Batsanov, A. S.; Bryce, M. R.; Petty, M. C. *J. Mater. Chem.* **2002**, *12*, 173. (c) O'Brien, D.; Bleyer, A.; Lidzey, D. G.; Bradley, D. D. C.; Tsutsui, T. *J. Appl. Phys.* **1997**, *82*, 2662.

(13) (a) Bettenhausen, J.; Strohriegl, P.; Brütting, W.; Tokuhisa, H.; Tsutsui, T. *J. Appl. Phys.* **1997**, *82*, 4957. (b) Noda, T.; Ogawa, H.; Noma, N.; Shirota, Y. *Adv. Mater.* **1997**, *9*, 239. (c) Noda, T.; Ogawa, H.; Noma, N.; Shirota, Y. *J. Mater. Chem.* **1999**, *9*, 2177.

(14) (a) Kraft, A. *Liebigs Ann.* **1997**, *7*, 1463. (b) Bettenhausen, J.; Strohriegl, P. *Adv. Mater.* **1996**, *8*, 507. (c) Bettenhausen, J.; Greczmiel, M.; Jandke, M.; Strohriegl, P. *Synth. Met.* **1997**, *91*, 223.

(15) Yeh, H.-C.; Lee, R.-H.; Chan, L.-H.; Lin, T.-Y. J.; Chen, C.-T.; Balasubramaniam, E.; Tao, Y.-T. *Chem. Mater.* **2001**, *13*, 2788.

(16) Bube, R. H. *Photoelectronic Properties of Semiconductors*; Cambridge University Press: Cambridge, 1992.

(17) Alam, M. M.; Jenekhe, S. A. *J. Phys. Chem. B* **2001**, *105*, 2479.

(18) (a) Parker, I. D.; Pei, Q.; Marrocco, M. *Appl. Phys. Lett.* **1994**, *65*, 1272. (b) Zhang, C.; von Seggern, H.; Pakbaz, K.; Kraabel, B.; Schmidt, H.-W.; Heeger, A. J. *Synth. Met.* **1994**, *62*, 35. (c) Zhang, C.; von Seggern, H.; Kraabel, B.; Schmidt, H.-W.; Heeger, A. J. *Synth. Met.* **1995**, *72*, 185. (d) Johnson, G. E.; McGrane, K. M.; Stolka, M. *Pure Appl. Chem.* **1995**, *67*, 175.

(19) Ranganathan, S.; Muraleedharan, K. M.; Rao, C. H. C.; Vairamani, M.; Karle, I. L.; Gilardi, R. D. *Chem. Commun.* **2001**, 2544.

(20) (a) Sauer, J.; Huisgen, R.; Sturm, H. J. *Tetrahedron* **1960**, *11*, 241. (b) Finnegan, W. G.; Henry, R. A.; Lofquist, R. *J. Am. Chem. Soc.* **1958**, *80*, 3908. (c) Ried, W.; Aboul-Fetouh, S. *Tetrahedron* **1988**, *44*, 3399.

(21) Meyer, E.; Joussef, A. C.; Gallardo, H. *Synthesis* **2003**, 899.

(22) (a) Revell, J. D.; Ganesan, A. *Chem. Commun.* **2004**, 1916. (b) Rozina, D. S.; Nesterenko, L. T.; Vainshtein, Y. I. *Zh. Obshch. Khim.* **1958**, *28*, 2878.

(23) (a) Dubey, A. K.; Sangwan, N. K. *Proc. Natl. Acad. Sci., India, Sec. A: Phys. Sci.* **2000**, *70*, 361. (b) Zhong, H.; Xu, E.; Zeng, D.; Du, J.; Sun, J.; Ren, S.; Jiang, B.; Fang, Q. *Org. Lett.* **2008**, *10*, 709. (c) Rekkas, S. A.; Rodios, N. A.; Alexandrou, N. E. *Synthesis* **1986**, 411. (d) Naito, K.; Watanabe, Y.; Egusa, S. *Jpn. J. Appl. Phys., Part 1* **1999**, *38*, 2792.

(24) Huisgen, R.; Sauer, J.; Sturm, H. J.; Markgraf, J. H. *Chem. Ber.* **1960**, *93*, 2106.

(25) Zafiropoulos, N. A.; Choi, E.-J.; Dingemans, T.; Lin, W.; Samulski, E. T. *Chem. Mater.* **2008**, *20*, 3821.

(26) Tolosa, J.; Zucchero, A. J.; Bunz, U. H. F. *J. Am. Chem. Soc.* **2008**, *130*, 6498.

(27) The calculations were carried out by using the package software of CAChe developed by Oxford Molecular Ltd. and Fujitsu Ltd.

(28) (a) Doroshenko, A. O.; Kyrychenko, A. V.; Waluk, J. *J. Fluoresc.* **2000**, *10*, 41. (b) Doroshenko, A. O.; Kirichenko, A. V.; Mitina, V. G.; Ponomaryov, O. A. *J. Photochem. Photobiol., A: Chem.* **1996**, *94*, 15. (c) Doroshenko, A. O.; Kyrychenko, A. V.; Baumer, V. N.; Verezubova, A. A.; Ptyagina, L. M. *J. Mol. Struct.* **2000**, *524*, 289. (d) For other discussion about the Stokes shift of twisted ground-state molecules, see Heimel, G.; Daghoferm, M.; Gierschner, J.; List, E. J. W.; Grimsdale, A. C.; Müllen, K.; Beljonne, D.; Brédas, J.-L.; Zojer, E. *J. Chem. Phys.* **2005**, *122*, 054501.

(29) Estimated against the energy level of 4.8 eV for ferrocence/ferrocenium. For references, see (a) Pommerehne, J.; Vestweber, H.; Guss, W.; Mahrt, R. F.; Bässler, H.; Porsch, M.; Daub, J. *Adv. Mater.* **1995**, *7*, 551. (b) Liu, Y.; Liu, M. S.; Jen, A. K.-Y. *Acta Polym.* **1999**, *50*, 105.

(30) (a) Hino, Y.; Kajii, H.; Ohmori, Y. *Jpn. J. Appl. Phys., Part 1* **2005**, *44v*, 2790. (b) Negres, R. A.; Gong, X.; Ostrowski, J. C.; Bazan, G. C.; Moses, D.; Heeger, A. J. *Phys. Rev. B: Condens. Matter.* **2003**, *68*, 115209. (c) Hu, B.; Yang, Z.; Karasz, F. E. *J. Appl. Phys.* **1994**, *76*, 2419.

(31) (a) Zhang, F.; Zhao, S.; Zhao, D.; Jiang, W.; Li, Y.; Yuan, G.; Zhu, H.; Xu, Z. *Phys. Scr.* **2007**, *75*, 407. (b) Lee, R.-H.; Hsu, H.-F.; Chan, L.-H.; Chen, C.-T. *Polymer* **2006**, *47*, 7001.

(32) Negres, R. A.; Gong, X.; Moses, D.; Heeger, A. J. *Trends Opt. Photon.* **2003**, *88*, CWA12/1−CWA12/3.

(33) Benson-Smith, J. J.; Wilson, J.; Dyer-Smith, C.; Mouri, K.; Yamaguchi, S.; Hideyuki Murata, H.; Nelson, J. *J. Phys. Chem. B* **2009**, *113* (22), 7794.

(34) (a) Poelman, D.; Van Meirhaeghe, R. L.; Laflère, W. H.; Cardon, F. *J. Phys. D: Appl. Phys.* **1992**, *25*, 1010. (b) Saito, S.; Tsutsui, T.; Era, M.; Takada, N.; Adachi, C.; Hamada, Y.; Wakimoto, T. *Proc. SPIE* **1993**, *1910*, 212.

(35) Kulkarni, A. P.; Jenekhe, S. A. *J. Phys. Chem. C* **2008**, *112*, 5174.

(36) Rusalov, M. V.; Druzhinin, S. I.; Uzhinov, B. M. *J. Fluoresc.* **2004**, *14*, 193.

JP9093063